Cancer Cell
Article

Targeted Disruption of Heparan Sulfate Interaction with Hepatocyte and Vascular Endothelial Growth Factors Blocks Normal and Oncogenic Signaling

Fabiola Cecchi,[1] Deborah Pajalunga,[2,3,6] C. Andrew Fowler,[2,7] Aykut Üren,[4] Daniel C. Rabe,[1] Benedetta Peruzzi,[1,8] Nicholas J. MacDonald,[3,9] Davida K. Blackman,[3,10] Stephen J. Stahl,[5] R. Andrew Byrd,[2] and Donald P. Bottaro[1,*]
[1]Urologic Oncology Branch, National Cancer Institute, Bethesda, MD 20892-1501, USA
[2]Macromolecular NMR Section, Structural Biophysics Laboratory, Frederick National Laboratory for Cancer Research, Frederick, MD 21702-1201, USA
[3]EntreMed, Inc., Rockville, MD 20850, USA
[4]Lombardi Comprehensive Cancer Center, Georgetown University Medical Center, Washington, DC 20057-1469, USA
[5]Protein Expression Laboratory, National Institute of Arthritis and Musculoskeletal and Skin Diseases, National Institutes of Health, Bethesda, MD 20892-2775, USA
[6]Present address: Department of Cell Biology and Neuroscience, Higher Institute of Health, Viale Regina Elena, 299, 00161 Rome, Italy
[7]Present address: Medical NMR Facility, Carver College of Medicine, University of Iowa, B291 CBRB, Iowa City, IA 52242, USA
[8]Present address: DAI Laboratory, SODc General Laboratory, AOU-Careggi, University of Florence, Largo Brambilla 3-50134 Florence, Italy
[9]Present address: Laboratory of Malaria Immunology and Vaccinology, NIAID, National Institutes of Health, Rockville, MD 20892-8252, USA
[10]Present address: ProMetic BioTherapeutics, Inc., Rockville, MD 20850, USA
*Correspondence: dbottaro@helix.nih.gov
http://dx.doi.org/10.1016/j.ccr.2012.06.029

SUMMARY

Hepatocyte growth factor (HGF) and vascular endothelial cell growth factor (VEGF) regulate normal development and homeostasis and drive disease progression in many forms of cancer. Both proteins signal by binding to receptor tyrosine kinases and heparan sulfate (HS) proteoglycans on target cell surfaces. Basic residues comprising the primary HS binding sites on HGF and VEGF provide similar surface charge distributions without underlying structural similarity. Combining three acidic amino acid substitutions in these sites in the HGF isoform NK1 or the VEGF isoform VEGF165 transformed each into potent, selective competitive antagonists of their respective normal and oncogenic signaling pathways. Our findings illustrate the importance of HS in growth factor driven cancer progression and reveal an efficient strategy for therapeutic antagonist development.

INTRODUCTION

Heparan sulfate (HS) glycosaminoglycans (GAGs) are complex polysaccharides present on cell surfaces and in extracellular matrices that modulate cell growth and differentiation, and in turn, embryogenesis, angiogenesis, and homeostasis (reviewed in Sarrazin et al., 2011). Their extended conformation and high negative charge enhance tissue integrity, and their inherent complexity provides selective yet substantial protein binding capacity (Sarrazin et al., 2011). Protein binding enables the formation of growth factor gradients during development and reservoirs for factors needed rapidly for tissue repair and regeneration in adults (Sarrazin et al., 2011). Cell surface HS proteoglycans form ternary complexes with growth factors and their receptors, enhancing complex stability and signaling (Sarrazin et al., 2011; Mohammadi et al., 2005).

Significance

Heparan sulfate (HS) proteoglycans are widely expressed, structurally diverse biopolymers that modulate many important protein-protein interactions. Hepatocyte growth factor (HGF) and vascular endothelial cell growth factor (VEGF) regulate development and homeostasis and drive tumorigenesis, tumor angiogenesis, and metastasis in many forms of cancer. We show that targeted disruption of specific HS binding residues in HGF and VEGF yields selective competitive inhibitors of these pathways. The similar roles of HS in enabling receptor activation, in the absence of underlying structural similarity, suggest that this occurs through convergent evolutionary adaptation to the common binding partner, HS. Our results reveal an efficient strategy for the development of antagonists of these and potentially other HS binding growth factors with widespread involvement in cancer.

Hepatocyte growth factor (HGF) and vascular endothelial cell growth factor (VEGF) bind HS and regulate development and homeostasis (Ferrara, 2004; Matsumoto and Nakamura, 1996; Michalopoulos, 2007) and drive tumor growth, angiogenesis, and metastasis in many cancers (Boccaccio and Comoglio, 2006; Ferrara, 2004; Peschard and Park, 2007). HGF induces growth, motility, and morphogenesis in a variety of cell types via the Met receptor kinase (Peschard and Park, 2007). VEGF-A is an essential regulator of angiogenesis (Ferrara, 2004) that stimulates growth, motility, and tubulogenesis in vascular endothelial cells through the receptor kinases VEGFR1 (Flt-1) and VEGFR2 (Flk-1, kinase insert domain receptor [KDR]) and the coreceptors neuropilin-1 (NRP1) and NRP2 (Ferrara, 2004; Favier et al., 2006; Gluzman-Poltorak et al., 2000).

The *HGF* and *VEGF* genes encode multiple isoforms. Mature HGF is a plasminogen-like protein that comprises an amino-terminal heavy chain with four kringle motifs and a carboxyl-terminal light chain with a serine protease-like domain (Matsumoto and Nakamura, 1996). Two truncated HGF isoforms also exist: the shorter of these retains HGF activities at modestly reduced potency and consists of the amino-terminal (N) domain linked to kringle 1 (NK1) (Stahl et al., 1997). Within NK1, N contains the HS binding site (Hartmann et al., 1998; Kinosaki et al., 1998; Lietha et al., 2001; Mizuno et al., 1994; Okigaki et al., 1992; Sakata et al., 1997; Zhou et al., 1998, 1999), and K1 contains the primary Met binding site (Lokker et al., 1994; Rubin et al., 2001).

VEGF-A pre-mRNA splicing yields multiple VEGF-A isoforms, primarily VEGF121, VEGF165, and VEGF189 (Ferrara, 2004). These contain the same binding sites for VEGFR1 and R2, but differ in HS binding capacity by the presence or absence of domains encoded by exon 6 and exon 7 (Robinson and Stringer, 2001). Exon 7- and exon 8-encoded domains enable VEGF-A to bind NRP1 (Appleton et al., 2007; Ferrara, 2004). Unlike VEGF165 and VEGF189, VEGF121 lacks HS binding and is freely diffusible (Carmeliet et al., 1999). HS binding has significant impact on VEGF-A biology: mice engineered to express only VEGF121 display defective microvessel branching and lethality shortly after birth (Carmeliet et al., 1999). Yet, even VEGF121 signaling is HS dependent: similar to fibroblast growth factors (FGFs) and HGF, HS facilitates VEGF signaling through interactions with both ligand and receptor (Lyon et al., 2002; Mohammadi et al., 2005; Rubin et al., 2001; Sarrazin et al., 2011). Thus, complete disruption of HS function in VEGF signaling is likely to mimic the embryonic lethality associated with homozygous deletions of VEGF, VEGFR, or the HS proteoglycan perlecan (Ferrara, 2004; Sarrazin et al., 2011).

Basic residues critical for HS binding have been identified in HGF and VEGF165 (Chirgadze et al., 1999; Krilleke et al., 2007; Lietha et al., 2001; Ultsch et al., 1998; Zhou et al., 1998, 1999). Combined alanine substitutions in the VEGF165 HS binding site resulted in reduced binding to NRP1 and VEGFR1 (Krilleke et al., 2007). Alanine substitutions in the HS binding site of HGF (Kinosaki et al., 1998) or NK1 (Lokker et al., 1994; Sakata et al., 1997) resulted in modest functional change. Negative charge substitutions that more effectively disrupt HS binding distinguished functionally relevant sites in HGF over earlier studies (Hartmann et al., 1998), so this strategy was used to further define the importance of HS binding for Met and VEGFR signaling.

RESULTS

Substituted NK1 Forms Have Normal Folding and Met Binding but Diminished HS Binding and Signaling

The highly conserved N domain residues K60, K62, and R73 form the primary HS binding site in HGF and R76, K78, R35, and R36 contribute secondarily (Chirgadze et al., 1999; Lietha et al., 2001; Ultsch et al., 1998; Zhou et al., 1998, 1999; Table S1 available online). Within the HS binding domain of VEGF165, residues R123, R124, and R159 are also highly conserved and critical for heparin binding (Krilleke et al., 2007; Table S1). Although HGF and VEGF have neither significant sequence identity nor similarity in peptide backbone fold, the tripartite HS binding sites in both show a similar distribution of positive surface charge (Figure S1).

Expression plasmids were constructed that substituted acidic for basic residues to disrupt the surface charge distribution on NK1: R73E (designated 1S), K60E/K62E (2S), and K60E/K62E/R73E (3S). Substituted and wild-type (WT) NK1 proteins were expressed and purified to >99% homogeneity (Figure S2). To confirm proper folding of the substituted proteins, their structures were compared with WT by nuclear magnetic resonance (NMR) spectrometry (Figure 1). Minor shifts in the pattern of two-dimensional ^{1}H-^{15}N correlation spectra for substituted proteins overlaid on NK1 WT spectra clustered near the substitution sites, indicating minimal perturbation of the three-dimensional structure in the substituted proteins.

Competitive binding experiments using ruthenium (Ru) tagged NK1 WT protein bound to immobilized heparin with displacement by untagged WT or 3S proteins showed that binding by the 3S form was 10-fold lower than WT ($p < 0.001$; Figure 2A). The IC_{50} for WT was consistent with prior estimates of NK1- and NK2-heparin binding (Hartmann et al., 1998; Rubin et al., 2001). Elution of the substituted proteins from a heparin affinity column by a NaCl gradient also showed reduced binding relative to WT, most severely in NK1 3S, reinforcing prior evidence that residues 60, 62, and 73 are sites of HS interaction (Table S2).

Saturation binding of tagged NK1 WT and 3S proteins to a Met ectodomain-Ig fusion protein in the presence of HS oligomer (4.2 kDa) or HS tetramer (1.2 kDa) produced similar results (Figures 2B and 2C), indicating that Met binding was unchanged, as anticipated. Competitive displacement of HGF by NK1 WT or 3S also yielded IC_{50} values of ~1 nM (data not shown). Saturation binding of tagged NK1 3S to the Met-Ig protein was unaffected by the absence of HS (Figure 2B, triangles); in contrast, NK1 WT binding to Met-Ig in the absence of HS was significantly compromised (Figure 2C, triangles). Heparin (18 kDa) substituted effectively for either HS form in enhancing NK1 WT-Met binding (data not shown). Together, these results suggest that masking the positive surface charge of residues 60, 62, and 73 with bound HS in NK1 WT improves its Met binding affinity and that this was achieved artificially in NK1 3S by the negative charge substitutions.

Disruption of the primary HS binding site in NK1 diminished its biological activity in cultured cells. Ligand-induced Met autophosphorylation in human epithelial (184B5) cells was lower in cells treated with NK1 1S or 2S proteins relative to NK1 WT or HGF (data not shown) and undetectable in cells treated with NK1 3S protein (Figure 2D). Ligand-stimulated cell migration (Figure 2E) and mitogenesis (Figure 2F) revealed similar patterns

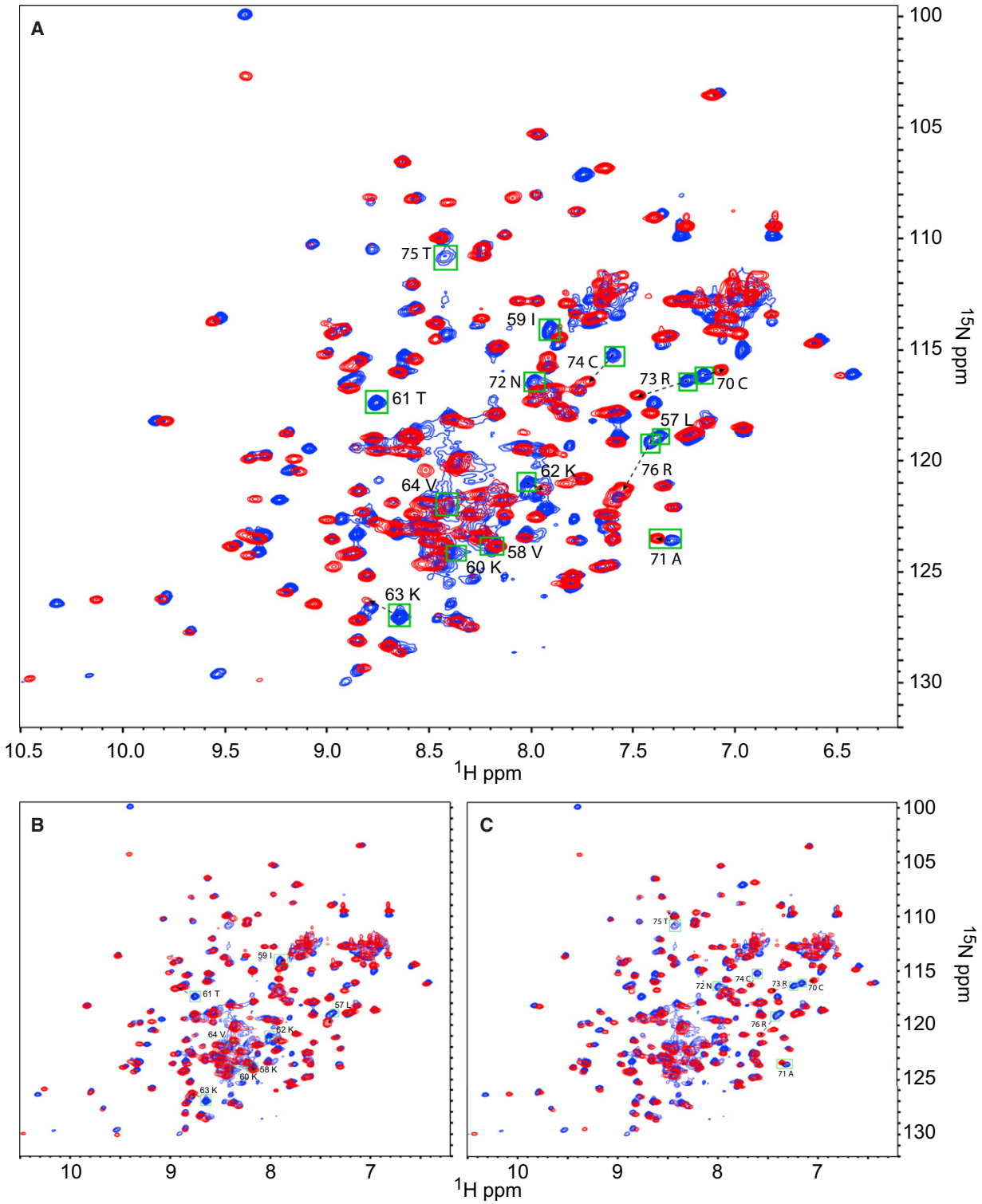

Figure 1. NMR Analysis of NK1 Proteins

^{1}H-^{15}N correlation spectra for substituted NK1 proteins (red) superimposed on NK1 WT spectra (blue).

(A) NK1 3S.

(B) NK1 2S.

(C) NK1 1S.

Spectra that are shifted in the substituted proteins are labeled in (A), (B), and (C).

See also Figure S1 and Table S1.

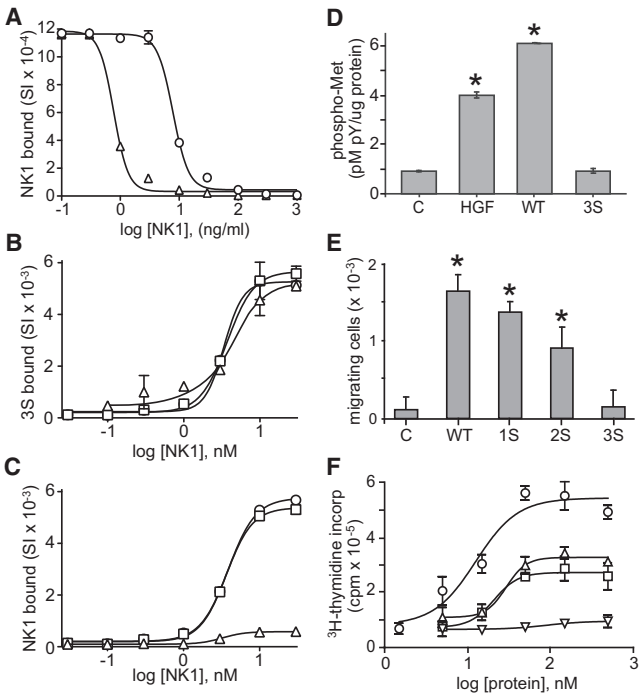

Figure 2. NK1 3S Has Reduced HS Binding and Normal Met Binding and Fails to Activate Met Signaling

(A–C) Competitive displacement of Ru tagged NK1 WT from immobilized heparin by untagged NK1 WT (triangles) or 3S (circles) (A). Saturation binding of Ru tagged NK1 3S (B) or NK1 WT (C) to Met ectodomain-Ig in the absence (triangles) or presence of HS oligomer (circles) or HS tetramer (squares). For (A), (B), and (C) values are mean signal intensity (SI) ± SD (n = 3).

(D) Mean Met activation (phospho-Met [pM] per total protein [ug] ± SD; n = 3) in 184B5 cells left untreated ("C") or treated with HGF (1 nM), NK1 WT (5 nM), or NK1 3S (5 nM) for 20 min. Met content was equivalent in all samples. Asterisks indicate significant differences from control ($p < 0.01$).

(E) Mean number of 184B5 cells (± SD; n = 3) migrating in response to treatment with NK1 WT or substituted NK1 proteins (7 nM each) in 24 hr. Asterisks indicate significant differences from control ($p < 0.01$).

(F) Mean DNA synthesis values ([^{3}H]thymidine incorporation cpm ± SD; n = 3) in 184B5 cells after 16 hr treatment with NK1 WT or substituted proteins at the indicated concentrations: WT (circles); 1S (triangles); 2S (squares); and 3S (inverted triangles).

See also Figure S2 and Table S2.

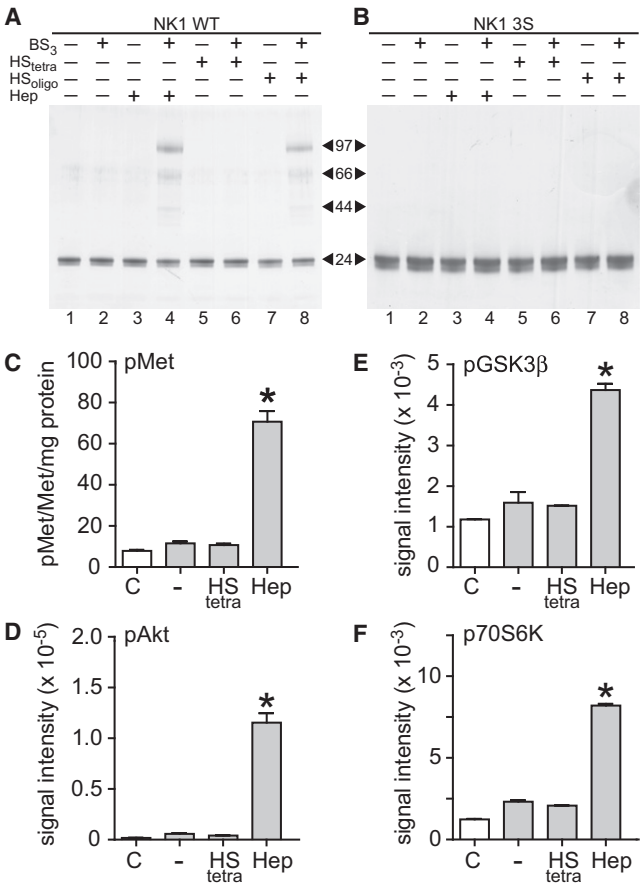

Figure 3. Long HS Polymers Promote NK1 Clustering, Met Activation, and Signaling

(A and B) Purified NK1 WT (A), or NK1 3S proteins were incubated alone or with BS_3 crosslinker in the absence or presence of heparin (Hep), HS oligomers (HS_{oligo}), or HS tetramers (HS_{tetra}) before analysis by SDS-PAGE and immunoblotting (B). Arrows between (A) and (B) indicate the masses of NK1 monomer (24 kDa) and NK1 multimers.

(C–F) The activation states of Met (mean phospho-Met/Met/total protein ± SD; n = 3; C), Akt (D), GSK3β (E), or p70S6K (F) in serum-deprived CHO 745 cells that were untreated (unfilled bars, "C") or treated with NK1 WT (200 pM; gray bars) in the absence (–) or presence of HS tetramer (HS_{tetra}) or heparin (Hep). Values for (D–F) are mean signal intensity units (± SD; n = 3). Asterisks indicate significant differences from control ($p < 0.01$).

of functional compromise among the substituted NK1 forms: the 1S and 2S proteins showed reduced activity ($p < 0.01$), and the 3S protein was inactive.

NK1-HS Binding Enables NK1 Clustering, Met Activation, and Signaling

Loss of signaling by NK1 3S despite native Met binding implied that HS binding enabled a critical step in Met activation. HGF and NK1 are monomers in solution, and it is thought that long HS chains capable of binding several HGF molecules promote and stabilize ligand clustering, and in turn, the clustering of ligand-receptor complexes (Chirgadze et al., 1999; Gherardi et al., 2006; Lietha et al., 2001; Hartmann et al., 1998; Rubin et al., 2001; Schwall et al., 1996; Tolbert et al., 2007; Zhou et al., 1999). Consistent with this concept, 18 kDa heparin or 4.2 kDa HS oligomer supported NK1 WT multimer formation detected after covalent affinity crosslinking, SDS-PAGE, and immunoblotting (Figure 3A, lanes 4 and 8). HS tetramers (1.2 kDa) unable to bind more than one NK1 molecule (Lyon et al., 2002) did not support NK1 WT multimer formation (Figure 3A, lane 6). The masses of the observed NK1 WT oligomers corresponded to dimers, trimers, and tetramers of NK1 (Figure 3A). As anticipated, HS-NK1 3S complexes were not detected (Figure 3B).

The impact of HS chain length on NK1-driven Met signaling was investigated using Chinese hamster ovary (CHO) 745 cells, which lack HS (Sarrazin et al., 2011). NK1-Met binding and NK1 clustering on cell surfaces were found to be HS dependent in CHO 745 (Sakata et al., 1997). Consistent with this, and other studies (Lyon et al., 2002, 2004), Met TK activation (Figure 3C) and consequent activation of Akt (Figure 3D), glycogen synthase kinase 3β

(GSK3β) (Figure 3E), and p70S6K (Figure 3F) by NK1 WT in this cell line was enhanced by added 18 kDa heparin. In contrast, added 1.2 kDa HS tetramer did not enhance NK1 WT signaling (Figures 3C–3F), despite enabling high affinity NK1-Met binding (Figure 2C). These observations suggest that the clustering of NK1 afforded by longer HS chains stabilized NK1-Met complex oligomerization, and, in turn, Met signaling. The relative order in which ligand-HS, ligand-Met, and Met-HS binding events occur is unknown and may be dictated by the relative abundance of HS and Met on target cells. We note that HS tetramer enabled modest mitogen-activated protein kinase (MAPK) activation by HGF (Lyon et al., 2002); as suggested by Stamos et al. (2004), the HGF light chain may contribute to HGF/Met/HS complex dimerization through homotypic interactions between light-chain protomers.

NK1 3S Is a Potent, Selective Competitive Antagonist of NK1 and HGF Signaling

The properties of the NK1 3S protein suggested that it might competitively antagonize HGF activity. Indeed, addition of 3S protein to HGF- and NK1-treated cells resulted in dose-dependent inhibition Met kinase activation in normal cells (Figure 4A, circles and squares). The IC_{50} values for 3S inhibition of Met activation by HGF and NK1 WT were 6 nM, 10-fold more potent than the Met antagonist PHA665752 (IC_{50} = 60 nM; Figure 4A, triangles). NK1 WT-induced DNA synthesis was also inhibited by 3S protein, with >90% inhibition at 10-fold molar excess 3S over WT NK1 (Figure 4B, circles).

CD44 variants containing exon 6 (v6) are implicated in oncogenic Met signaling (Orian-Rousseau et al., 2002), and those containing exon 3 are often modified with HS and promote HGF-Met interaction (van der Voort et al., 1999; Wielenga et al., 2000). CD44 variants containing both exons occur frequently in colon and prostate cancer-derived cell lines, such as HT29 and PC3M, respectively, and in colon and prostate carcinomas where their expression correlates with poor prognosis (van der Voort et al., 1999; Wielenga et al., 2000). We analyzed Met-CD44 association to determine if NK1 3S-Met binding affected this process. Met-CD44 association was induced by HGF or NK1 WT in HT29 cells (Figure 4C, lanes 2 and 3) and by HGF in PC3M cells (Figure 4D, lane 2), but not by NK1 3S in either cell line (Figure 4C, lane 4; Figure 4D, lane 6). In PC3M, NK1 3S antagonized HGF-induced Met-CD44 association in a dose-dependent manner, while PHA665752 was less effective (Figure 4D, lanes 2–5 versus lanes 7–9).

Oncogenic autocrine HGF/Met signaling occurs frequently in glioblastoma (Boccaccio and Comoglio, 2006) and drives tumorigenicity in the glioblastoma-derived cell line U87 MG. Stable expression of NK1 3S in U87 MG cells significantly reduced proliferation relative to cells expressing NK1 WT or empty vector (Figure 4E). HGF and Met protein levels were comparable in the three cell lines, as were the levels of NK1 WT and 3S proteins (Figures S3A–S3E). U87 MG cells do not express NK1 mRNA, thus reduced growth resulted from NK1 3S inhibition of endogenous HGF signaling.

We extended our initial analysis of NK1 3S inhibition of cell motility (Figure 2E) using the Madin-Darby Canine Kidney (MDCK) cell scatter assay (Figure 4F). NK1 3S had no intrinsic scatter activity (Figure 4F, third panel from left); inhibition of HGF-induced scatter was dose-dependent and complete at 50-fold molar excess (Figure 4F, right three panels).

NK1 3S also blocked anchorage independent growth by U87 MG cells (Figure 4G). U87 MG cells grow robustly in soft agar, (Figure 4G, left panel), but cells expressing NK1 3S failed to form colonies under identical conditions (Figure 4G, second panel from left). Colony formation was also suppressed by adding purified NK1 3S protein to the medium, with ~50% inhibition by 70 nM 3S and complete blockade by 300 nM relative to controls (Figure 4G, third and fourth panels from left); similar levels of inhibition were observed for PHA665752 (Figure 4G, right two panels).

The Met selectivity of NK1 3S antagonism was confirmed using the endothelial hybrid cell line EA.hy 926, which expresses both Met and KDR. Cells were stimulated with either NK1 WT or VEGF165 in the presence or absence of 10-fold molar excess NK1 3S, and the activation levels of Met, Akt, GSK3β, and p70S6K were measured by 2-site immunoassays (Figures S3F–S3I). NK1 3S did not activate Met or downstream effectors (Figures S3F–S3I, left versus right white bars). NK1 WT activated Met, Akt, and its targets relative to control cells (Figures S3F–S3I, left white versus left gray bars), and this signaling cascade was completely suppressed by added excess NK1 3S (Figures S3F–S3I, right gray bars). In contrast, although VEGF165 fully activated the Akt pathway, excess NK1 3S had no effect (Figures S3F–S3I, left versus right black bars). Similar results were observed for VEGF165 activation of the MAPK pathway kinases pERK-1/2, pJNK, and pp38 MAPK in the presence or absence of NK1 3S (data not shown).

NK1 3S Inhibits HGF Signaling, Tumor Growth, and Metastasis In Vivo

NK1 3S antitumor activity was first assessed by xenograft studies of transfected U87 MG cell lines in severe combined immunodeficiency (SCID)/beige mice (Figure 5A). Animals receiving the U87 MG/NK1 WT cell line started to develop tumors in 5 days (Figure 5A, squares), and tumor growth rate was twice that of the control cell line (Figure 5A, circles), consistent with the additive effects of ectopic NK1 WT and endogenous HGF. In contrast, tumor growth in animals receiving U87 MG/NK1 3S cells was not measurable before 50 days (Figure 5A, triangles). Like U87 MG, the human leiomyosarcoma-derived cell line SK-LMS-1 has autocrine HGF/Met activation. SK-LMS-1 cells were transfected with plasmids for NK1 WT, NK1 3S, or with empty vector, and cell clones were selected for equivalent expression of endogenous HGF and Met and ectopic NK1 WT and NK1 3S proteins (Figures S3A–S3E). Again, NK1 WT expression accelerated tumor growth (Figure 5B, squares), whereas NK1 3S expression reduced mean tumor volume by 75% after 68 days relative to controls (Figure 5B, triangles versus circles; $p < 0.001$). Tumors resected from these mice displayed equivalent Met content among the three groups (not shown); Met activation was highest in NK1 WT transfectant tumors (Figure 5C, black bar), significantly lower in tumors from controls (Figure 5C, gray bar), and lowest in tumors from the NK1 3S implanted group (Figure 5C, white bar; $p < 0.001$).

HGF/Met signaling is a critical contributor to tumor metastasis (Boccaccio and Comoglio, 2006). NK1 3S was tested in the B16 murine melanoma model of induced metastasis, where

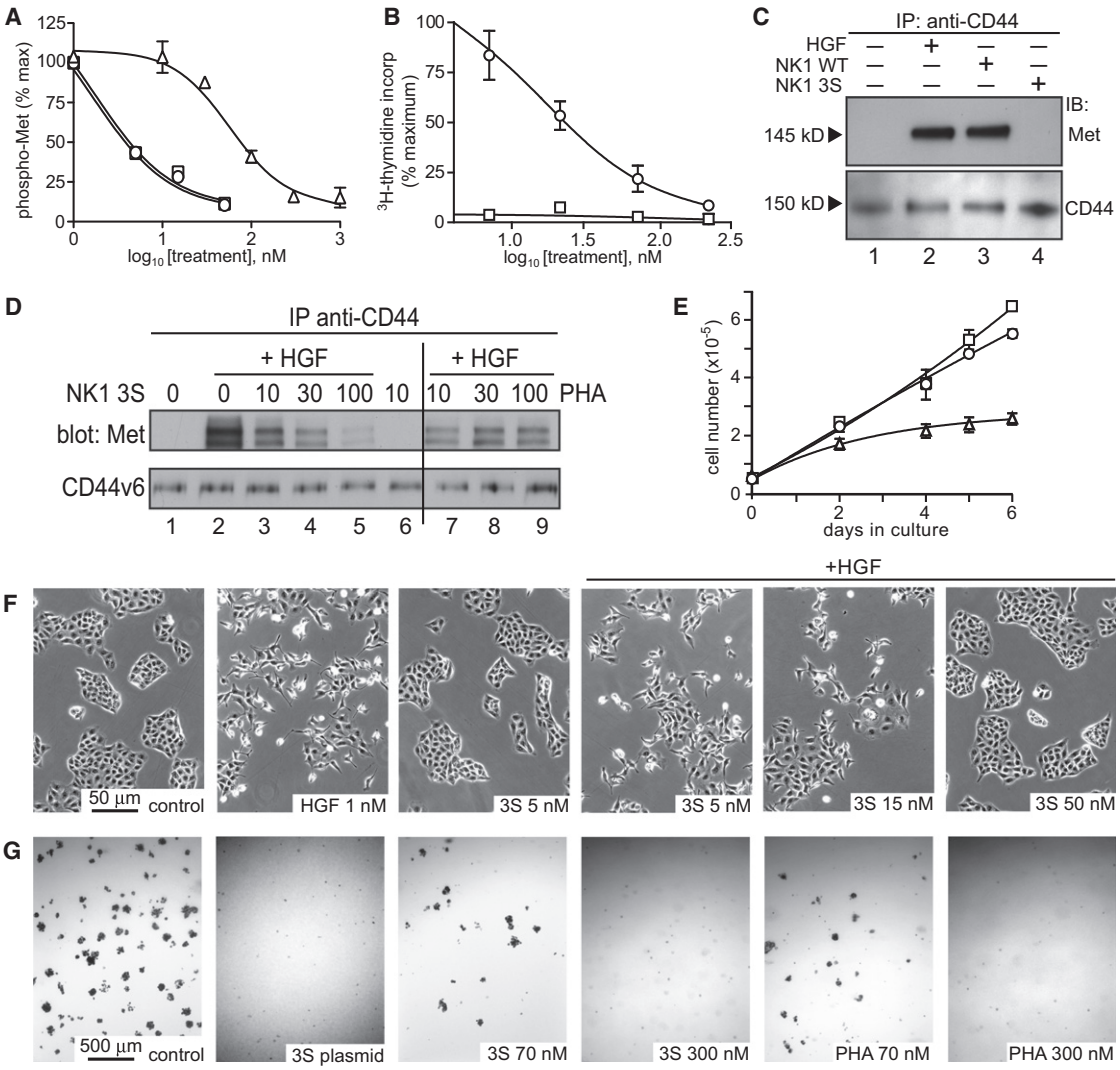

Figure 4. NK1 3S Is a Potent Antagonist of NK1 and HGF Signaling

(A) Mean Met activation level (% maximum ± SD; n = 3) in 184B5 cells treated with HGF (1 nM; circles) or NK1 WT (5 nM; squares) and with increasing concentrations of NK1 3S. HGF-stimulated cells were treated with PHA665752 (triangles) over the same dose range in parallel.

(B) Mean DNA synthesis level (% maximum [^{3}H]thymidine incorporation ± SD; n = 3) in 184B5 cells treated with NK1 WT and NK1 3S (circles), or in cells treated with NK1 3S alone (squares) at the indicated doses.

(C) Met-CD44 association in HT29 cells incubated with NK1 3S (5 nM), NK1 WT (5 nM), or HGF (1 nM) as indicated, in the presence of DTSSP prior to immunoprecipitation with anti-CD44, SDS-PAGE, and immunoblotting with anti-Met (upper panel) or anti-CD44 (lower panel).

(D) Met-CD44 association in PC3M cells treated with HGF (1 nM) and DTSSP in the absence or presence of NK1 3S or PHA665752 (PHA) at the indicated concentrations (nM) prior to immunoprecipitation with anti-CD44, SDS-PAGE, and immunoblotting with anti-Met (upper panel) or anti-CD44 (lower panel).

(E) Proliferation of U87 MG cells (mean cell number ± SD; n = 3) expressing NK1 WT (squares), NK1 3S (triangles), or empty vector (circles).

(F) NK1 3S antagonism of HGF-stimulated MDCK cell scatter. Unstimulated control cells or cells treated with HGF or NK1 3S at the indicated concentrations (left three panels). HGF-stimulated cells treated with NK1 3S at the indicated concentrations (right three panels).

(G) Soft agar colony formation by U87 MG cells transfected with vector (control) or NK1 3S cDNA (3S plasmid) or control cells treated with NK1 3S protein or PHA665752 (PHA) at the indicated concentrations.

See also Figure S3.

endogenous HGF drives metastatic colonization. B16 cells expressing luciferase (B16-luc) were used to enable tumor burden assessment by optical imaging. Metastasis in animals injected with B16-luc cells expressing NK1 3S was compared with metastasis in animals injected with empty vector cells and with metastasis in animals injected with the empty vector cells and then treated by daily intraperitoneal (i.p.) injection of purified NK1 3S protein at 50 mg/kg (Figure 5D). Metastatic burden rose rapidly in the mice receiving empty vector cells (Figure 5D, circles), whereas mice receiving 3S plasmid bearing cells (Figure 5D, squares) or control cells and i.p. treatment with 3S protein (Figure 5D, triangles) showed few, if any, metastases by study

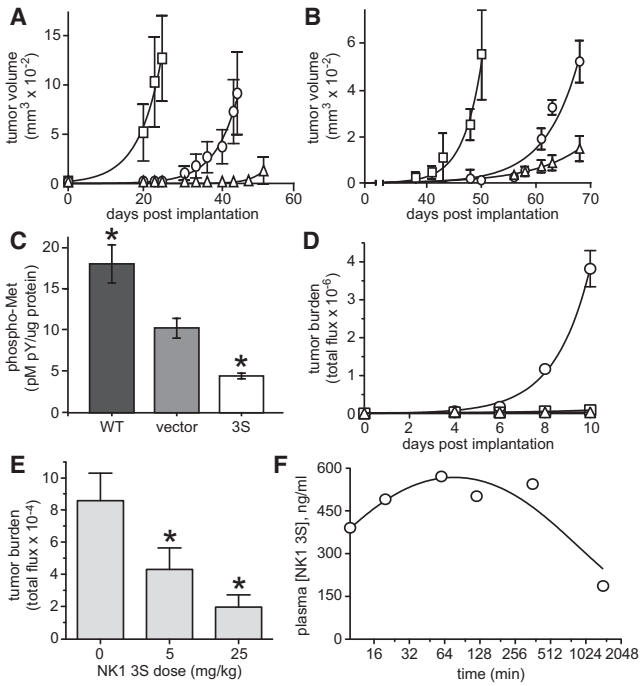

Figure 5. NK1 3S Inhibits HGF-Driven Tumor Growth, Metastasis, and Met Kinase Activation In Vivo

(A) Mean tumor volume (± SD) in mice (n = 6/group) implanted with U87 MG transfectants expressing NK1 WT (squares), NK1 3S (triangles), or empty vector (circles) at the indicated days postimplantation.

(B) Mean tumor volume (± SD) in mice (n = 6/group) implanted with clonal SK-LMS-1-derived cell lines expressing NK1 WT (squares), NK1 3S (triangles), or empty vector (circles) at the indicated days postimplantation.

(C) Mean Met activation level (phospho-Met/Met/total protein ± SD; n = 3) in SK-LMS-1 tumors derived from SK-LMS-1 cells expressing NK1 WT (black), empty vector (gray), and NK1 3S (unfilled). Asterisks indicate significant differences from vector control ($p < 0.01$).

(D) Mean metastatic burden (total photon flux ± SD) over time in mice (n = 10/group) injected via tail vein with B16-luc cells transfected with empty vector (circles) or NK1 3S (squares) or injected with empty vector cells and then treated on day 2 and thereafter with NK1 3S (50 mg/kg) by daily i.p. injection (triangles).

(E) Mean metastatic burden (total photon flux ± SD on day 27 postimplantation) in mice (n = 10/group) implanted subcutaneously with PC3M-luc cells and treated on day 5 and daily thereafter with NK1 3S protein by i.p. injection at 5 or 25 mg/kg or treated with vehicle alone.

(F) Mean plasma NK1 3S protein concentration (ng/ml, n = 2) in mice (n = 6) measured at the indicated times following a single i.p. injection of NK1 3S at 50 mg/kg.

See also Figure S4.

termination ($p < 0.001$). Lung specimens from each group examined ex vivo at study termination for melanin-producing colonies were consistent with the imaging results (data not shown). The B16-luc melanoma model was also used for a preliminary dose-ranging study where mice received i.p. injections of NK1 3S protein at day 2 post-tail vein injection and daily thereafter for 15 days at 5, 25, and 50 mg/kg (Figure S4). Significant metastatic suppression was observed at every NK1 3S dose ($p < 0.001$).

The antimetastatic efficacy of NK1 3S was also evaluated in the PC3M spontaneous metastasis model (Figure 5E). The PC3M cells used in these studies also expressed luciferase for metastatic burden assessment. Palpable subcutaneous primary tumors developed within 5 days after cell implantation; mice then received daily i.p. injections of purified NK1 3S protein at 5 or 25 mg/kg, or vehicle alone. Primary tumor growth was measured at regular intervals using calipers, and metastatic burden was measured by imaging at study termination. Interestingly, NK1 3S treatment had no significant effect on primary tumor growth in this model (data not shown); however, a significant and dose-dependent inhibition of metastasis was observed, with 80% reduction at 25 mg/kg ($p < 0.01$; Figure 5E).

Analysis of NK1 3S pharmacokinetics in mice (n = 6) showed that plasma NK1 level peaked between 1 and 3 hr after a single i.p. injection (50 mg/kg) and declined thereafter (Figure 5F). Plasma NK1 3S concentration 24 hr postinjection was ~150 ng/ml or ~300-fold over typical murine plasma HGF levels. Mice treated daily with this dose for 10 days showed no weight loss, lethargy, or other signs of toxicity. Mice (n = 5) treated on this dose and schedule, but not implanted with tumor cells, displayed normal clinical blood chemistry, differential blood cell count, and hematocrit values; full necropsy analysis of all tissues and organs showed no signs of toxicity or abnormality (data not shown).

VEGF165 3S Is a Potent Competitive VEGF Antagonist

To determine whether the strategy used to transform NK1 from agonist to antagonist could be generalized, we generated a cDNA encoding opposite charge substitution at the critical HS binding residues identified by Krilleke et al. (2007) in VEGF165 (R123E/R124E/R159E or VEGF165 3S). Plasmids encoding vector alone, VEGF165 WT or VEGF165 3S, were stably transfected into HEK293 cells that were engineered previously to express 2.5×10^6 VEGFR2 per cell (293/KDR; Backer et al., 2005). VEGF165 WT expression in these cells was expected to result in autocrine KDR activation and transformation, whereas VEGF165 3S was expected to lack KDR activating ability and have no effect on phenotype. Ectopic VEGF protein production by transfectants was measured using a 2-site immunoassay with a 1.5 pM detection limit. Marker selected cultures of WT transfectants produced ~1.0 ng/ml/24 hr VEGF165 protein in conditioned media, 3S transfectants produced ~2.5 ng/ml/24 hr, and VEGF protein was undetectable in vector control media (Figure 6A). Like VEGF165 WT, VEGF 3S dimers and monomers of expected mass were detected under nonreducing and reducing conditions, respectively (Figure 6B). Saturation binding of VEGF165 3S to KDR in vitro (Figure 6C, squares; K_D ~19 pM) was equivalent to VEGF165 WT binding (Figure 6C, circles; K_D ~23 pM) and consistent with published values (Ferrara, 2004).

KDR autophosphorylation in each cell line was measured after 24 hr of serum deprivation (Figure 6D). The basal KDR phosphorylation level in empty vector transfectants (Figure 6D, white bar) was similar to that of the parental cell line (not shown) and 3S transfectants (Figure 6D, dark gray bar). In contrast, WT transfectant basal KDR phosphorylation level was 4-fold higher than control or 3S (Figure 6D, light gray bar; $p < 0.001$). The KDR autophosphorylation level of the vector transfectant after 20 min exposure to added VEGF165 protein (2.5 nM) is shown for reference (Figure 6D, black bar).

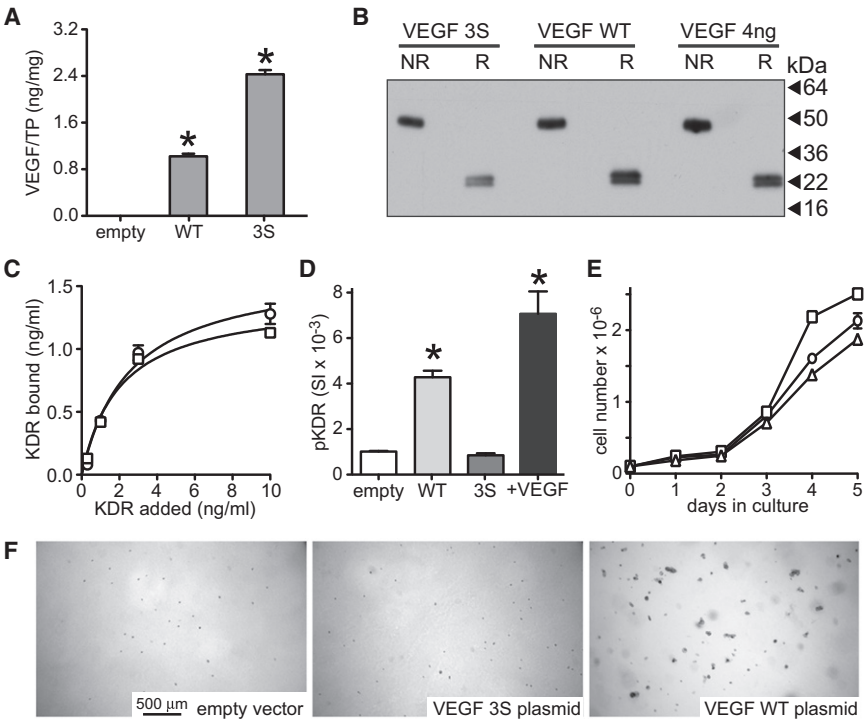

Figure 6. VEGF165 3S Dimer Binds KDR Normally but Does Not Signal

(A) Mean VEGF165 content (ng/mg total cell protein ± SD; n = 3) in 24 hr conditioned media prepared from 293/KDR cells transfected with empty vector (empty), VEGF165 WT (WT), or VEGF165 3S (3S). Asterisks indicate significant differences from vector control ($p < 0.01$).

(B) VEGF165 3S (VEGF 3S; left) and VEGF165 WT (VEGF WT; middle) proteins in 24 hr conditioned media prepared from 293/KDR transfectants and purified recombinant VEGF165 protein (VEGF 4 ng; right) after SDS-PAGE under nonreducing (NR) and reducing (R) conditions and immunoblotting with anti-VEGF. Migration of molecular mass standards (kDa) is indicated by arrows.

(C) Saturation binding of KDR ectodomain-IgG fusion protein to VEGF165 WT (squares) or VEGF165 3S proteins (circles) in vitro. Values are mean KDR bound (ng/ml ± SD; n = 3).

(D) Mean phospho-KDR level (signal intensity ± SD; n = 3) in 293/KDR cells transfected with empty vector (empty; unfilled bar), VEGF165 WT (WT; light gray bar), VEGF165 3S (3S; dark gray bar), or empty vector cells treated with purified VEGF165 WT protein (2.5 nM) for 20 min (+VEGF; black bar). Asterisks indicate significant differences from empty vector control ($p < 0.01$).

(E) Growth rate (mean cell number ± SD; n = 3) of cultured 293/KDR cells transfected with empty vector (circles), VEGF165 WT (squares), or VEGF165 3S (triangles).

(F) Soft agar colony formation by 239/KDR cells transfected with empty vector, (left), VEGF 3S (middle), or VEGF WT (right).

Consistent with the levels of KDR activation among the transfectants, significant differences in cell proliferation rate were observed from day 3 onward: WT transfectants (Figure 6E, squares) grew significantly faster than the vector control (Figure 6E, circles) or 3S transfectants (Figure 6E, triangles; $p < 0.001$ between WT and control or WT and 3S for days 3–5). These results indicated that WT transfectants, but not 3S transfectants, had acquired autocrine VEGF signaling, even though 3S protein production was twice that of WT. In soft agar colony formation assays, empty vector and 3S transfectants grew modestly, if at all (Figure 6F, left and middle panels), whereas WT transfectants grew robustly (Figure 6F, right panel). All of these results indicated loss of signaling by VEGF165 3S despite native KDR binding.

VEGF165 3S also antagonized VEGF165 WT signaling in intact cells. Concentrated conditioned media harvested from 3S transfectants was added to 293/KDR cells in the presence of purified VEGF165 WT protein and phospho-KDR levels were measured (Figures 7A and 7B). Since the conditioned media could contain other inhibitors of KDR activation, VEGF165 3S was selectively removed from the media by immunodepletion with anti-VEGF antibody. A mock immunodepletion was performed in parallel using a nonspecific antibody and the VEGF165 3S content of the anti-VEGF, and mock-immunodepleted media was measured (Figure 7A). VEGF 3S levels in nonimmunodepleted and mock-immunodepleted media were similar (1.93 and 1.89 ng/mg total cell protein, respectively; Figure 7A, white bars), while immunodepletion with anti-VEGF removed 95% of the 3S protein (0.096 ng/mg total cell protein; Figure 7A, gray bar). VEGF was not detected in media from empty vector transfectants before or after immunodepletion (Figure 7A, right). KDR autophosphorylation stimulated by purified VEGF165 protein (10 ng/ml) in serum-deprived 293/KDR cells (Figure 7B) was inhibited modestly by VEGF-immunodepleted media (Figure 7B, circles), but mock-immunodepleted media showed significant, dose-dependent inhibition, with >80% inhibition by media containing 2.5-fold molar excess VEGF 3S protein (Figure 7B, triangles). In soft agar colony formation assays, robust growth of 293/KDR cells transfected with VEGF165 WT (Figure 7C, upper left panel) was inhibited in a dose-dependent manner by the VEGFR inhibitor pazopanib (Figure 7C, middle and right upper panels), providing additional evidence that colony formation was driven by autocrine VEGF/KDR signaling. VEGF165 3S protein added at 0.06, 0.15, and 0.6 nM also resulted in significant, dose-dependent inhibition (Figure 7C, lower panels).

Analysis of the spectrum of VEGF 3S antagonism showed that VEGF165 3S inhibited placenta growth factor (PlGF)-induced Akt activation (phospho-Akt/total Akt) in EA.hy 926 cells, which express VEGFR1 and R2, with potency similar to pazopanib (Figure 7D). In contrast, VEGF 3S did not block Akt activation induced by VEGF-D in SCC-25 cells, which express VEGFR1, R2, and R3 (Figures S5A and S5B). Thus, the pattern of VEGF 3S inhibition followed the pattern of VEGF-A binding to VEGFR1 and R2 but not homodimers of VEGFR3, as anticipated (Ferrara, 2004).

VEGF165 3S antagonism was independent of NRP1-VEGF-A protein-protein interaction. NRP1 binds to the VEGF-A HS

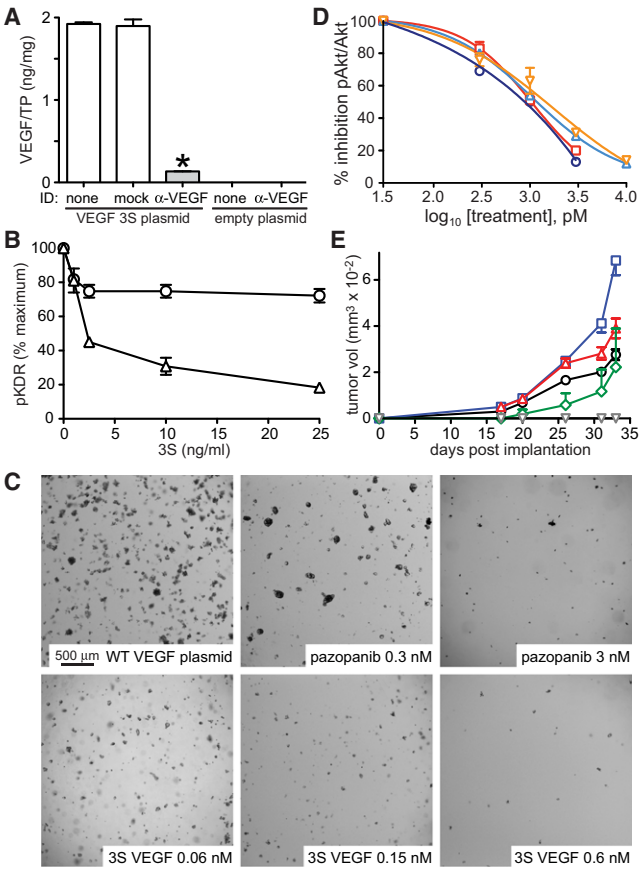

Figure 7. VEGF165 3S Antagonizes VEGFR Activation, Colony Formation, and Tumorigenesis

(A) VEGF165 content in media conditioned by 293/KDR cells transfected with VEGF165 3S (left) or empty plasmid (right), before ("none") or after immunodepletion by anti-VEGF-A ("α-VEGF") or an unrelated control antibody ("mock"), expressed as mean ng/mg total protein ± SD (n = 3). Asterisk indicates significant difference from media prior to immunodepletion ($p < 0.01$).

(B) Phospho-KDR levels (% maximum, ± SD; n = 3) in serum-deprived 293/KDR cells treated with VEGF165 WT (10 ng/ml) in the presence of concentrated conditioned media from 293/KDR VEGF 3S transfectants that were immunodepleted using a nonspecific control antibody (triangles) or anti-VEGF (circles). The x axis indicates VEGF165 3S concentration (ng/ml) in conditioned media before immunodepletion.

(C) Soft agar colony formation by 239/KDR cells expressing VEGF165 WT (upper left panel), cells treated with the indicated concentrations of pazopanib (upper middle and right panels), or cells treated with media containing the indicated concentrations of VEGF165 3S (lower panels).

(D) Dose-dependent inhibition of VEGF- or PlGF-induced Akt activation (mean % inhibition phospho-Akt/total Akt ± SD) in EA.hy 926 cells. VEGF 3S blocked Akt activation by VEGF-A (dark blue circles) or PlGF (red squares) with potency similar to pazopanib (light blue triangles and yellow inverted triangles, respectively).

(E) Mean tumor volume (mm^3 ± SD) in mice (n = 5/group) implanted with 293/KDR cells (3×10^6 cells per animal) expressing VEGF165 3S (gray inverted triangles), VEGF165 WT (blue squares), or empty vector (black circles) at the indicated times postimplantation. Other groups were implanted with a mixture of empty vector cells and VEGF165 WT transfectants at 1.5×10^6 cells each (red triangles) or a mixture of VEGF165 WT and VEGF165 3S transfectants at 1.5×10^6 cells each (green diamonds).

See also Figure S5.

binding domain primarily at R165 and secondarily at K147, E152, and E155 (Parker et al., 2012), i.e., to a surface opposite that of HS (Figure S5C). Crosslinking studies further showed that VEGF165 WT and VEGF165 3S bound similarly to NRP1 in vitro (Figure S5D). Functionally, VEGF165 3S antagonized VEGF signaling similarly in 293/KDR derived cells (Figures 7B, 7C, and 7E), which lack NRP1 (Figure S5E, lanes 4–6), and in EA.hy 926 cells (Figure 7D), which are NRP1 positive (Figure S5E, lane 2). The NRP1 present in our experiments was not HS modified, which is thought to promote NRP1 multimerization and, in turn, NRP1-VEGFR2 binding and signaling (Shintani et al., 2006). Like NK1, we found that heparin promoted clustering of VEGF165 WT, but not of VEGF165 3S (Figure S5F). Thus, if HS-modified NRP1 enhances VEGF signaling in part by promoting VEGF clustering, VEGF165 3S would be expected to antagonize that process.

VEGF 3S Inhibits VEGF-Driven Tumor Growth and Angiogenesis In Vivo

To test whether VEGF165 3S protein could antagonize KDR-driven tumorigenicity in mice, animals were implanted subcutaneously with VEGF165 WT transfected 293/KDR cells (3×10^6 per animal), with the same number of VEGF165 3S transfected cells or with a suspension containing 1.5×10^6 cells of each line. Additional control groups received the empty vector 293/KDR cells (3×10^6 per animal) or the empty vector cells combined with VEGF WT transfectants at 1.5×10^6 cells each. The latter group indicated the growth rate of tumors arising from 1.5×10^6 VEGF WT transfectants in the presence of "neutral" cells providing the same initial mass; a growth rate below this threshold in the group implanted with VEGF WT + VEGF 3S transfectants could be attributed to inhibition of VEGF WT-driven tumor growth by VEGF165 3S. Indeed, VEGF WT transfected 293/KDR cells formed tumors fastest (Figure 7D, blue squares), whereas VEGF 3S transfectants did not form tumors prior to study termination (Figure 7D, gray inverted triangles), and animals implanted with the WT + 3S cell mix (Figure 7D, green diamonds) formed tumors at a significantly lower rate than the control WT + empty vector group (Figure 7D, red triangles) throughout the study ($p < 0.05$).

Tumorigenesis by the parental cell line, despite its inability to grow in soft agar, indicated that it was driven by host VEGF. This conclusion is supported by prior work where the generation of knockin mice expressing a humanized form of VEGF-A was needed to overcome incomplete suppression of human tumor xenograft growth by antihuman VEGF-A antibodies that did not block murine VEGF activity (Gerber et al., 2007). Therefore, the failure of the 3S transfectants to form tumors indicates VEGF 3S antagonism of tumorigenesis driven by murine VEGF. Moreover, significant inhibition of tumor growth by VEGF165 3S in animals receiving the WT + 3S transfectant cell mix indicates antagonism of the combined impact of paracrine murine VEGF and autocrine human VEGF.

Tumor angiogenesis was also significantly blocked in mice receiving VEGF 3S transfected cells (Figure 8). Immunohistochemisty using anti-CD34 showed that the extent of tumor vascularization, from highest to lowest, was 293/KDR/WT VEGF transfectants alone (Figure 8A), 293/KDR/WT VEGF cells + vector transfected 293/KDR cells mixed 1:1 (Figure 8B), vector

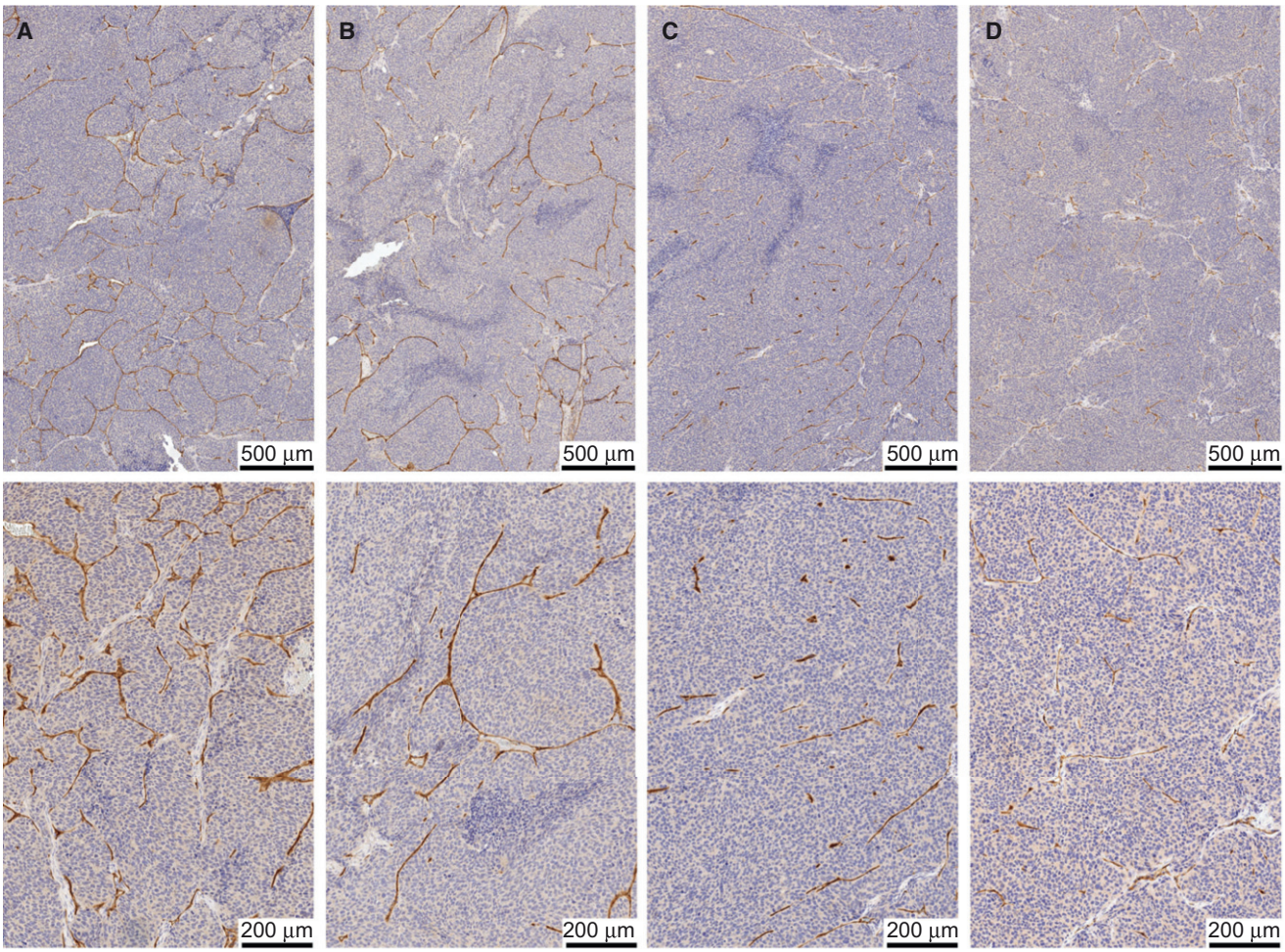

Figure 8. VEGF165 3S Antagonizes VEGF-Driven Tumor Angiogenesis

Murine CD34 immunohistochemical analysis (low magnification above, higher magnification below) of tumors from animal groups as described in Figure 7. (A) 293/KDR/VEGF WT cell tumors; (B) 293/KDR/VEGF WT + control 293/KDR cell (1:1) tumors; (C) control 293/KDR cell tumors; (D) 293/KDR/VEGF WT + 293/KDR/VEGF 3S cell (1:1) tumors.

transfectants alone (Figure 8C), and 293/KDR/WT VEGF + 293/KDR/3S VEGF transfectants mixed 1:1 (Figure 8D). This pattern is consistent with tumor angiogenesis driven by both autocrine human and paracrine murine VEGF (Figures 8A and 8B) relative to tumor angiogenesis driven by murine VEGF alone (Figure 8C) and with substantial inhibition of tumor angiogenesis by VEGF 3S (Figure 8D).

Histopathology analysis indicated that the tumors formed by 293/KDR cell transfectants (vector, VEGF WT, VEGF WT + vector, VEGF WT + VEGF 3S) were uniformly carcinoma. Full necropsy analysis of all tissue and organs showed no signs of toxicity or damage in any tissue from mice implanted with 293/KDR transfectants.

DISCUSSION

Our work builds on several prior studies showing that HS-HGF interaction is critical for HGF signaling (Hartmann et al., 1998; Lietha et al., 2001; Sakata et al., 1997; Schwall et al., 1996; Zioncheck et al., 1995). The loss of biological activity by combined substitution of K60, K62, and R73 with acidic residues identifies this surface region as essential for NK1 biological signaling and implies that HS binding at secondary sites is insufficient for NK1 signaling. The partial loss of activity associated with substitutions at 73 and 60/62 suggests that each contribute to HS interactions at this site. Our results further indicate that HS-NK1 interactions promote receptor activation and signaling by enhancing NK1-Met interaction and by stabilizing NK1 multimers, which may in turn facilitate receptor clustering, kinase activation, and effector recruitment (Gherardi et al., 2006; Hartmann et al., 1998; Lietha et al., 2001; Sakata et al., 1997; Schwall et al., 1996; Tolbert et al., 2010).

We believe that three critical features define the mechanism of HGF inhibition by NK1 3S: (1) retention of optimal N domain-Met binding through negative charge substitutions in NK1 3S that mimic occupancy of the primary HS binding site; a prior report provides structural evidence to this effect (Tolbert et al., 2010), (2) repulsion of HS from the ligand-receptor complex by the negative charge substitutions, and (3) competitive displacement of HGF from Met by the native K1 domain of NK1 3S. We propose

that occupancy of the primary ligand binding site in Met without HS support of ligand-Met complex clustering and associated conformational changes results in a signaling blockade.

In addition to its value as a research tool, NK1 3S may have therapeutic potential. The critical role of HGF-Met signaling in a variety of human cancers has made Met an important anticancer drug target. Met blockade has been achieved using ATP binding site antagonists, neutralizing antibodies, decoy receptors, single-chain HGF derivatives (Cecchi et al., 2010), synthetic HS mimetics (Fuster and Esko, 2005), and engineered NK1 forms affecting the dimerization interface in K1 (Tolbert et al., 2010; Youles et al., 2008). Like the latter, NK1 3S blocks signaling by disrupting ligand dimer/multimer formation, but unlike those mutants it does so by blocking HS facilitation of that process. Each of these approaches has advantages as well as limitations. Our choice to develop NK1 instead of full-length HGF is based on the complexity of HGF protein and the technical obstacles this imposes on its manufacture. The challenges of administering large HGF-derived antagonists, such as NK4 and uncleavable pro-HGF, have been met by using viral vectors or naked DNA plasmids (Cecchi et al., 2010). These methods can provide sustained delivery but do not allow the level of control inherent in administering the encoded proteins. NK1 can be expressed in *P. pastoris* at yields high enough (>1 g/l) to be commercially tractable. Our results support the efficacy of systemically delivered NK1 3S protein as an antitumor and antimetastatic agent as well as its practicality as an alternative to larger HGF-derived antagonists.

We find that VEGF165 3S binds KDR-like VEGF165 WT protein, fails to induce KDR kinase activity, and antagonizes VEGF165 WT binding and signaling in vitro and in vivo. A critical distinction between VEGF165 3S and alanine substitutions made at these positions (Krilleke et al., 2007), or the VEGF isoform VEGF121, is that the opposite charge substitutions in VEGF 3S are designed to repel HS and thereby disrupt both ligand-HS and weaker receptor-HS interactions. The striking parallels in antagonism by 3S forms of NK1 and VEGF165 strengthen our assertion of a common role for HS in receptor activation and show that targeted disruption of critical HS binding sites is an antagonist development strategy that can be extended to other HS-binding growth factors. Consistent with findings for NK1, VEGF-HS interaction occurs through sulfated HS side-chains and three key VEGF residues, with secondary contributions from one or two others (Krilleke et al., 2007). The analogous roles of HS in NK1/Met and VEGF165/KDR signaling, in the absence of underlying structural similarity, suggests that this occurs through convergent evolution. Thus, any similarity in the spatial arrangement of the primary HS binding site surfaces themselves would be driven by adaptation to the common binding partner, HS, as opposed to a common ancestral protein sequence or structure.

The present understanding of KDR activation by VEGF165 and HS suggests a mechanistic basis for signaling antagonism by the targeted disruption of HS-ligand binding. The VEGF binding site in KDR encompasses IgG-like domains (D) 1–3: D2 contains primary contacts, and D1 and D3 contribute to overall binding affinity and specificity (Christinger et al., 2004; Fuh et al., 1998). Consistent with findings presented here for NK1, HS was found to be required for high-affinity binding of VEGF165 to KDR ectopically expressed in HS-negative CHO 745 cells (Dougher et al., 1997). Similar to Met (Rubin et al., 2001) and FGF receptors (Mohammadi et al., 2005), KDR also interacts directly with HS through at least one site located between D6 and D7 (Dougher et al., 1997). Recent structural studies of KIT, PDGFR, and VEGFR highlight the importance of homotypic receptor-receptor interaction domains in stabilizing receptor dimerization and kinase transactivation: direct contacts between D4 domains for KIT and D7 domains for KDR are enabled by ligand-induced conformational changes in the receptor ectodomain (Lemmon and Schlessinger, 2010; Tao et al., 2001; Yang et al., 2010). In these models, sequential binding events promote and incrementally stabilize HS-ligand-receptor aggregates capable of signaling. We hypothesize that VEGF165 first binds KDR D2; the weaker VEGF165 D1 and VEGF165 D3 interactions may be stabilized by HS-VEGF interaction and by HS-VEGF-KDR bridging at D6/D7. For VEGF165 3S, receptor binding at D2 should occur, but subsequent weaker interactions normally stabilized by HS and induced changes in receptor conformation could fail. VEGF-HS interactions may also induce conformational changes that enable the apposition of KDR D7 domains (Wijelath et al., 2010) and, in turn, homotypic interaction and kinase transactivation; VEGF165 3S is likely to disrupt such events. The role of NRP1 in VEGF signaling is complex, involving protein-protein interactions and protein-HS interactions when NRP1 is HS modified (Shintani et al., 2006). VEGF165 3S engages NRP1 via the former, but would be expected to disrupt the latter. Collectively, our observations underscore the importance of specific HS interactions in facilitating events after ligand binding, which are required for KDR activation, and expose their susceptibility to targeted disruption.

HS binding growth factors promote tumor growth, angiogenesis, and metastasis in a variety of human cancers. In addition to the strategy described here, oligosaccharide HS mimetics and modified heparin fragments can act as HS binding antagonists (Fuster and Esko, 2005). However, the complexity of HS GAGs challenges the development of potent and selective agents, and frequent alterations in HS GAG composition in tumors (Fuster and Esko, 2005) may render such agents less competitive for ligand binding. In contrast, opposite substitutions to critical HS binding residues in an otherwise wild-type protein ligand are simple to introduce, unaffected by tumor HS GAG composition, and inherently pathway selective. These features suggest that it may be an expedient and practical route for the development of antagonists of HS binding growth factors.

EXPERIMENTAL PROCEDURES

Reagents and Cell Culture

See Supplemental Information.

Plasmids for NK1 and VEGF165, Protein Expression, and Purification

NK1 proteins were produced in *E. coli* as described (Stahl et al., 1997). Plasmids for expression of NK1 3S, NK1 WT, VEGF165 WT, and VEGF165 3S under cytomegalovirus promoters possess their native signal peptide sequences and G418 resistance. Plasmids for *P. pastoris* expression of NK1 proteins were generated and protein purified as described in Supplemental Information.

NMR Structural Analysis

Isotope-labeled proteins were expressed *E. coli* in minimal media containing either $^{15}NH_4Cl$ or both $^{15}NH_4Cl$ and ^{13}C-labeled glucose. Triple-labeled

proteins ($^{15}N/^{13}C/^{2}H$) were prepared similarly, except the media contained 98% D_2O. ^{1}H-^{15}N correlation spectra for substituted and WT NK1 proteins were collected as described (Zhou et al., 1999). NK1 backbone resonance assignments were made using $^{15}N/^{13}C/^{2}H$-NK1 and standard triple resonance experiments.

Immunoassays and Binding Assays

Met, KDR, HGF, and VEGF content in cell lysates, tissue extracts, and conditioned media was determined using 2-site immunoassays developed for use with the Meso Scale Discovery (MSD) SectorImager 2400 plate reader; HGF and Met assays are described in Supplemental Information; other assays were from MSD. Met and KDR activation in cell lysates or tumor tissue extracts included parallel detection with antireceptor antibodies and specific antiphospho-receptor antibodies or 4G10 (Millipore).

Binding assays were also performed on the MSD platform. NK1 saturation binding to immobilized Met ectodomain-IgG fusion protein was measured using Ru tagged WT or 3S ligand. Displacement experiments included multiple untagged ligand concentrations in the presence of Ru tagged ligand. NK1-HS saturation binding to immobilized heparin-biotin was measured using Ru tagged NK1 WT or 3S proteins. KDR-Ig ectodomain saturation binding to immobilized VEGF165 WT or 3S was measured using Ru tagged anti-KDR. All measurements were made on triplicate samples. GraphPad Prism v5.0 was used for all statistical analyses. Additional details are included in Supplemental Information.

Cell Motility, Mitogenesis, and Colony Formation Assays

Cell motility in modified Boyden chambers and DNA synthesis by [^{3}H]thymidine incorporation were measured as described (Rubin et al., 2001). MDCK cell scatter was assessed as described (Stahl et al., 1997). U87 MG or 293/KDR derived cell line proliferation in quadruplicate wells of 6-well plates was measured by counting in a Cellometer (Nexcelom Bioscience). Assays for colony formation in soft agar were performed as described (Castagnino et al., 2000). Differences between mean values were determined by t test using GraphPad Prism v5.0.

Tumorigenesis, Metastasis, and Pharmacokinetic Assays

Experiments with SCID/beige mice were performed in accordance with National Institutes of Health (NIH) Guidelines for Care and Use of Laboratory Animals using protocols approved by the Institutional Animal Care and Use Committee of the Center for Cancer Research, National Cancer Institute. Details for all animal studies are included in Supplemental Information. Briefly, U87 MG, SK-LMS-1, or 293/KDR derived cell lines were injected subcutaneously into mice, and tumor volumes were calculated from caliper measurements. 293/KDR cell derived tumors were harvested at study termination for histopathology and immunohistochemical analysis of murine CD34 protein localization. B16-luc derived cells for induced metastasis studies were injected through the tail vein; in some studies, mice also received daily i.p. injections of purified NK1 3S (or vehicle) at doses indicated in the text. For spontaneous metastasis studies, PC3M-luc cells were implanted subcutaneously, and mice were treated by i.p. injection of vehicle or NK1 3S starting on day 5. Metastatic burden was determined by luciferase imaging. Plasma NK1 3S levels were measured in mice after a single i.p. injection of NK1 3S at the indicated times postinjection. NK1 protein was analyzed by SDS-PAGE and immunoblotting. Statistical analysis, curve fitting, and IC_{50} determinations were performed using GraphPad Prism v5.0.

SUPPLEMENTAL INFORMATION

Supplemental Information includes two tables, five figures, and Supplemental Experimental Procedures and can be found with this article online at http://dx.doi.org/10.1016/j.ccr.2012.06.029.

ACKNOWLEDGMENTS

This research was supported by the Intramural Research Program of the NIH, National Cancer Institute, Center for Cancer Research. We thank the late Dr. Ralph Schwall for recombinant Met-Ig fusion protein; Dr. Jeffrey Esko for CHO 745 cells; Drs. Dominic Esposito, Troy Taylor, and William Gillette for plasmid and protein production and purification; and Drs. Miriam Anver, Lawrence Sternberg, and Roberta Smith for pathology, immunohistochemistry analysis, and clinical chemistry analyses.

Received: October 18, 2011
Revised: April 4, 2012
Accepted: June 26, 2012
Published: August 13, 2012

REFERENCES

Appleton, B.A., Wu, P., Maloney, J., Yin, J., Liang, W.C., Stawicki, S., Mortara, K., Bowman, K.K., Elliott, J.M., Desmarais, W., et al. (2007). Structural studies of neuropilin/antibody complexes provide insights into semaphorin and VEGF binding. EMBO J. *26*, 4902–4912.

Backer, M.V., Gaynutdinov, T.I., Patel, V., Bandyopadhyaya, A.K., Thirumamagal, B.T., Tjarks, W., Barth, R.F., Claffey, K., and Backer, J.M. (2005). Vascular endothelial growth factor selectively targets boronated dendrimers to tumor vasculature. Mol. Cancer Ther. *4*, 1423–1429.

Boccaccio, C., and Comoglio, P.M. (2006). Invasive growth: a MET-driven genetic programme for cancer and stem cells. Nat. Rev. Cancer *6*, 637–645.

Carmeliet, P., Ng, Y.S., Nuyens, D., Theilmeier, G., Brusselmans, K., Cornelissen, I., Ehler, E., Kakkar, V.V., Stalmans, I., Mattot, V., et al. (1999). Impaired myocardial angiogenesis and ischemic cardiomyopathy in mice lacking the vascular endothelial growth factor isoforms VEGF164 and VEGF188. Nat. Med. *5*, 495–502.

Castagnino, P., Lorenzi, M.V., Yeh, J., Breckenridge, D., Sakata, H., Munz, B., Werner, S., and Bottaro, D.P. (2000). Neu differentiation factor/heregulin induction by hepatocyte and keratinocyte growth factors. Oncogene *19*, 640–648.

Cecchi, F., Rabe, D.C., and Bottaro, D.P. (2010). Targeting the HGF/Met signalling pathway in cancer. Eur. J. Cancer *46*, 1260–1270.

Chirgadze, D.Y., Hepple, J.P., Zhou, H., Byrd, R.A., Blundell, T.L., and Gherardi, E. (1999). Crystal structure of the NK1 fragment of HGF/SF suggests a novel mode for growth factor dimerization and receptor binding. Nat. Struct. Biol. *6*, 72–79.

Christinger, H.W., Fuh, G., de Vos, A.M., and Wiesmann, C. (2004). The crystal structure of placental growth factor in complex with domain 2 of vascular endothelial growth factor receptor-1. J. Biol. Chem. *279*, 10382–10388.

Dougher, A.M., Wasserstrom, H., Torley, L., Shridaran, L., Westdock, P., Hileman, R.E., Fromm, J.R., Anderberg, R., Lyman, S., Linhardt, R.J., et al. (1997). Identification of a heparin binding peptide on the extracellular domain of the KDR VEGF receptor. Growth Factors *14*, 257–268.

Favier, B., Alam, A., Barron, P., Bonnin, J., Laboudie, P., Fons, P., Mandron, M., Herault, J.P., Neufeld, G., Savi, P., et al. (2006). Neuropilin-2 interacts with VEGFR-2 and VEGFR-3 and promotes human endothelial cell survival and migration. Blood *108*, 1243–1250.

Ferrara, N. (2004). Vascular endothelial growth factor: basic science and clinical progress. Endocr. Rev. *25*, 581–611.

Fuh, G., Li, B., Crowley, C., Cunningham, B., and Wells, J.A. (1998). Requirements for binding and signaling of the kinase domain receptor for vascular endothelial growth factor. J. Biol. Chem. *273*, 11197–11204.

Fuster, M.M., and Esko, J.D. (2005). The sweet and sour of cancer: glycans as novel therapeutic targets. Nat. Rev. Cancer *5*, 526–542.

Gerber, H.P., Wu, X., Yu, L., Wiesmann, C., Liang, X.H., Lee, C.V., Fuh, G., Olsson, C., Damico, L., Xie, D., et al. (2007). Mice expressing a humanized form of VEGF-A may provide insights into the safety and efficacy of anti-VEGF antibodies. Proc. Natl. Acad. Sci. USA *104*, 3478–3483.

Gherardi, E., Sandin, S., Petoukhov, M.V., Finch, J., Youles, M.E., Ofverstedt, L.G., Miguel, R.N., Blundell, T.L., Vande Woude, G.F., Skoglund, U., and Svergun, D.I. (2006). Structural basis of hepatocyte growth factor/scatter factor and MET signalling. Proc. Natl. Acad. Sci. USA *103*, 4046–4051.

Gluzman-Poltorak, Z., Cohen, T., Herzog, Y., and Neufeld, G. (2000). Neuropilin-2 is a receptor for the vascular endothelial growth factor (VEGF) forms VEGF-145 and VEGF-165 [corrected]. J. Biol. Chem. *275*, 18040–18045.

Hartmann, G., Prospero, T., Brinkmann, V., Ozcelik, C., Winter, G., Hepple, J., Batley, S., Bladt, F., Sachs, M., Birchmeier, C., et al. (1998). Engineered mutants of HGF/SF with reduced binding to heparan sulphate proteoglycans, decreased clearance and enhanced activity in vivo. Curr. Biol. *8*, 125–134.

Kinosaki, M., Yamaguchi, K., Murakami, A., Ueda, M., Morinaga, T., and Higashio, K. (1998). Identification of heparin-binding stretches of a naturally occurring deleted variant of hepatocyte growth factor (dHGF). Biochim. Biophys. Acta *1384*, 93–102.

Krilleke, D., DeErkenez, A., Schubert, W., Giri, I., Robinson, G.S., Ng, Y.S., and Shima, D.T. (2007). Molecular mapping and functional characterization of the VEGF164 heparin-binding domain. J. Biol. Chem. *282*, 28045–28056.

Lemmon, M.A., and Schlessinger, J. (2010). Cell signaling by receptor tyrosine kinases. Cell *141*, 1117–1134.

Lietha, D., Chirgadze, D.Y., Mulloy, B., Blundell, T.L., and Gherardi, E. (2001). Crystal structures of NK1-heparin complexes reveal the basis for NK1 activity and enable engineering of potent agonists of the MET receptor. EMBO J. *20*, 5543–5555.

Lokker, N.A., Presta, L.G., and Godowski, P.J. (1994). Mutational analysis and molecular modeling of the N-terminal kringle-containing domain of hepatocyte growth factor identifies amino acid side chains important for interaction with the c-Met receptor. Protein Eng. *7*, 895–903.

Lyon, M., Deakin, J.A., and Gallagher, J.T. (2002). The mode of action of heparan and dermatan sulfates in the regulation of hepatocyte growth factor/scatter factor. J. Biol. Chem. *277*, 1040–1046.

Lyon, M., Deakin, J.A., Lietha, D., Gherardi, E., and Gallagher, J.T. (2004). The interactions of hepatocyte growth factor/scatter factor and its NK1 and NK2 variants with glycosaminoglycans using a modified gel mobility shift assay. Elucidation of the minimal size of binding and activatory oligosaccharides. J. Biol. Chem. *279*, 43560–43567.

Matsumoto, K., and Nakamura, T. (1996). Emerging multipotent aspects of hepatocyte growth factor. J. Biochem. *119*, 591–600.

Michalopoulos, G.K. (2007). Liver regeneration. J. Cell. Physiol. *213*, 286–300.

Mizuno, K., Inoue, H., Hagiya, M., Shimizu, S., Nose, T., Shimohigashi, Y., and Nakamura, T. (1994). Hairpin loop and second kringle domain are essential sites for heparin binding and biological activity of hepatocyte growth factor. J. Biol. Chem. *269*, 1131–1136.

Mohammadi, M., Olsen, S.K., and Ibrahimi, O.A. (2005). Structural basis for fibroblast growth factor receptor activation. Cytokine Growth Factor Rev. *16*, 107–137.

Okigaki, M., Komada, M., Uehara, Y., Miyazawa, K., and Kitamura, N. (1992). Functional characterization of human hepatocyte growth factor mutants obtained by deletion of structural domains. Biochemistry *31*, 9555–9561.

Orian-Rousseau, V., Chen, L., Sleeman, J.P., Herrlich, P., and Ponta, H. (2002). CD44 is required for two consecutive steps in HGF/c-Met signaling. Genes Dev. *16*, 3074–3086.

Parker, M.W., Xu, P., Li, X., and Vander Kooi, C.W. (2012). Structural basis for the selective vascular endothelial growth factor-A (VEGF-A) binding to neuropilin-1. J. Biol. Chem. *2012*, 7.

Peschard, P., and Park, M. (2007). From Tpr-Met to Met, tumorigenesis and tubes. Oncogene *26*, 1276–1285.

Robinson, C.J., and Stringer, S.E. (2001). The splice variants of vascular endothelial growth factor (VEGF) and their receptors. J. Cell Sci. *114*, 853–865.

Rubin, J.S., Day, R.M., Breckenridge, D., Atabey, N., Taylor, W.G., Stahl, S.J., Wingfield, P.T., Kaufman, J.D., Schwall, R., and Bottaro, D.P. (2001). Dissociation of heparan sulfate and receptor binding domains of hepatocyte growth factor reveals that heparan sulfate-c-met interaction facilitates signaling. J. Biol. Chem. *276*, 32977–32983.

Sakata, H., Stahl, S.J., Taylor, W.G., Rosenberg, J.M., Sakaguchi, K., Wingfield, P.T., and Rubin, J.S. (1997). Heparin binding and oligomerization of hepatocyte growth factor/scatter factor isoforms. Heparan sulfate glycosaminoglycan requirement for Met binding and signaling. J. Biol. Chem. *272*, 9457–9463.

Sarrazin, S., Lamanna, W.C., and Esko, J.D. (2011). Heparan sulfate proteoglycans. Cold Spring Harb. Perspect. Biol. *3*, 1–33.

Schwall, R.H., Chang, L.Y., Godowski, P.J., Kahn, D.W., Hillan, K.J., Bauer, K.D., and Zioncheck, T.F. (1996). Heparin induces dimerization and confers proliferative activity onto the hepatocyte growth factor antagonists NK1 and NK2. J. Cell Biol. *133*, 709–718.

Shintani, Y., Takashima, S., Asano, Y., Kato, H., Liao, Y., Yamazaki, S., Tsukamoto, O., Seguchi, O., Yamamoto, H., Fukushima, T., et al. (2006). Glycosaminoglycan modification of neuropilin-1 modulates VEGFR2 signaling. EMBO J. *25*, 3045–3055.

Stahl, S.J., Wingfield, P.T., Kaufman, J.D., Pannell, L.K., Cioce, V., Sakata, H., Taylor, W.G., Rubin, J.S., and Bottaro, D.P. (1997). Functional and biophysical characterization of recombinant human hepatocyte growth factor isoforms produced in Escherichia coli. Biochem. J. *326*, 763–772.

Stamos, J., Lazarus, R.A., Yao, X., Kirchhofer, D., and Wiesmann, C. (2004). Crystal structure of the HGF β-chain in complex with the Sema domain of the Met receptor. EMBO J. *23*, 2325–2335.

Tao, Q., Backer, M.V., Backer, J.M., and Terman, B.I. (2001). Kinase insert domain receptor (KDR) extracellular immunoglobulin-like domains 4-7 contain structural features that block receptor dimerization and vascular endothelial growth factor-induced signaling. J. Biol. Chem. *276*, 21916–21923.

Tolbert, W.D., Daugherty, J., Gao, C., Xie, Q., Miranti, C., Gherardi, E., Woude, G.V., and Xu, H.E. (2007). A mechanistic basis for converting a receptor tyrosine kinase agonist to an antagonist. Proc. Natl. Acad. Sci. USA *104*, 14592–14597.

Ultsch, M., Lokker, N.A., Godowski, P.J., and de Vos, A.M. (1998). Crystal structure of the NK1 fragment of human hepatocyte growth factor at 2.0 A resolution. Structure *6*, 1383–1393.

van der Voort, R., Taher, T.E., Wielenga, V.J., Spaargaren, M., Prevo, R., Smit, L., David, G., Hartmann, G., Gherardi, E., and Pals, S.T. (1999). Heparan sulfate-modified CD44 promotes hepatocyte growth factor/scatter factor-induced signal transduction through the receptor tyrosine kinase c-Met. J. Biol. Chem. *274*, 6499–6506.

Wielenga, V.J., van der Voort, R., Taher, T.E., Smit, L., Beuling, E.A., van Krimpen, C., Spaargaren, M., and Pals, S.T. (2000). Expression of c-Met and heparan-sulfate proteoglycan forms of CD44 in colorectal cancer. Am. J. Pathol. *157*, 1563–1573.

Wijelath, E., Namekata, M., Murray, J., Furuyashiki, M., Zhang, S., Coan, D., Wakao, M., Harris, R.B., Suda, Y., Wang, L., and Sobel, M. (2010). Multiple mechanisms for exogenous heparin modulation of vascular endothelial growth factor activity. J. Cell. Biochem. *111*, 461–468.

Yang, Y., Xie, P., Opatowsky, Y., and Schlessinger, J. (2010). Direct contacts between extracellular membrane-proximal domains are required for VEGF receptor activation and cell signaling. Proc. Natl. Acad. Sci. USA *107*, 1906–1911.

Youles, M., Holmes, O., Petoukhov, M.V., Nessen, M.A., Stivala, S., Svergun, D.I., and Gherardi, E. (2008). Engineering the NK1 fragment of hepatocyte growth factor/scatter factor as a MET receptor antagonist. J. Mol. Biol. *377*, 616–622.

Zhou, H., Mazzulla, M.J., Kaufman, J.D., Stahl, S.J., Wingfield, P.T., Rubin, J.S., Bottaro, D.P., and Byrd, R.A. (1998). The solution structure of the N-terminal domain of hepatocyte growth factor reveals a potential heparin-binding site. Structure *6*, 109–116.

Zhou, H., Casas-Finet, J.R., Heath Coats, R., Kaufman, J.D., Stahl, S.J., Wingfield, P.T., Rubin, J.S., Bottaro, D.P., and Byrd, R.A. (1999). Identification and dynamics of a heparin-binding site in hepatocyte growth factor. Biochemistry *38*, 14793–14802.

Zioncheck, T.F., Richardson, L., Liu, J., Chang, L., King, K.L., Bennett, G.L., Fügedi, P., Chamow, S.M., Schwall, R.H., and Stack, R.J. (1995). Sulfated oligosaccharides promote hepatocyte growth factor association and govern its mitogenic activity. J. Biol. Chem. *270*, 16871–16878.